Journal of Alloys and Compounds 769 (2018) 92–95

Contents lists available at ScienceDirect

Journal of Alloys and Compounds

journal homepage: http://www.elsevier.com/locate/jalcom

Letter

Double-shell CeO_2:Yb, Er@SiO_2@Ag upconversion composite nanofibers as an assistant layer enhanced near-infrared harvesting for dye-sensitized solar cells

Keywords:
CeO_2:Yb,Er@SiO_2@Ag
Upconversion luminescence
Near-infrared absorption
Assistant layer
Dye-sensitized solar cells

A B S T R A C T

Double-shell CeO_2:Yb,Er@SiO_2@Ag upconversion composite nanofibers are synthesized by electrospinning and subsequent process. CeO_2:Yb,Er@SiO_2@Ag nanofibers show high upconversion luminescence property due to the coating of amorphous SiO_2 and the surface plasmon resonance effect of Ag nanoparticles. CeO_2:Yb,Er@SiO_2@Ag nanofibers act as an assistant layer in dye-sensitized solar cells (DSSCs) and enhance the photoelectric conversion efficiency (PCE) to 8.17%. The photocurrent-voltage characteristic is obtained under 980 nm laser as illumination light source. In addition, the absorption of the incident photon-to-current conversion efficiency curve in 900–1000 nm near-infrared light confirms that the introduction of the upconversion nanomaterial broadens the absorption range, improves the utilization rate of the sunlight and increases the PCE of DSSCs.

1. Introduction

The dye-sensitized solar cells (DSSCs), owing to their relatively good efficiency, easy manufacturing processing, and low cost, have garnered much attention since 1991 [1]. The main problem that limits the photoelectric conversion efficiency (PCE) of DSSCs is low absorption for the infrared and near-infrared (NIR) light, which occupies 43% of the solar spectrum. Photon upconversion provides an alternative approach to resolve this limitation utilizing NIR light absorber [2–4]. Therefore, one straightforward way to increase the PCE of DSSCs is adopted the suitable dye to broaden the sunlight harvesting range, but this kind of dye always is expensive and poor stability [5–8]. Moreover, the inorganic rare-earth doped $NaYF_4$ and Y_2O_3 nanomaterials are usually used as the upconversion materials, which are introduced into the DSSCs for adsorbing NIR light [9–14]. Cerium dioxide (CeO_2) has the stable crystalline field for the upconversion progress. Furthermore, it has a suitable energy band gap matching with TiO_2 and good light scattering effect, which lead to the wide-spread use of CeO_2 as an assistant component in DSSCs. A few research focus on rare-earth ion doped CeO_2 as an upconversion assistant layer in DSSCs [15–18].

In this work, we designed and synthesized double-shell CeO_2:Yb,Er@SiO_2@Ag upconversion composite nanofibers (UCNFs). Under the assistance of SiO_2 layer and Ag nanoparticles (NPs), CeO_2:Yb,Er@SiO_2@Ag UCNFs display the excellent upconversion luminescence performance. The use of CeO_2:Yb,Er@SiO_2@Ag UCNFs as assistant materials for improvement of the NIR light harvesting in DSSCs reach a PCE as high as 8.17%.

2. Materials and methods

In our work, the agents were acquired from Sinopharm Chemical Reagent Co. Ltd. (China). All reagents were analytical grade and received without further purification. The details for synthesizing CeO_2:Yb,Er@SiO_2@Ag UCNFs, sensitized DSSCs and characterization are shown in Supporting Information (SI).

3. Results and discussions

Fig. 1a illustrates the preparation progress of CeO_2:Yb,Er@SiO_2@Ag UCNFs. Firstly, CeO_2:Yb,Er nanofibers as fluorescence center are synthesized *via* electrospinning and calcination. Secondly, the SiO_2 layers are coated on the surface of CeO_2:Yb,Er nanofibers by hydrolysis of TEOS to form the core-shell CeO_2:Yb,Er@SiO_2 nanofibers. Lastly, Ag NPs *in situ* grow on the surface of SiO_2 by microwave irradiation to obtain double-shell CeO_2:Yb,Er@SiO_2@Ag UCNFs. SEM and TEM images of the intermediate or final products were shown in Fig. 1b–j. The composite nanofibers have a dimeter about 150 nm with the about 15 nm thickness of SiO_2 and the Ag NPs is about 10 nm. The HRTEM images (Fig. 1k–l), SAED pattern (Fig. 1m), and element mapping images (Fig. 1n–s) prove the well crystallinity, the composite structure and the hypodispersion of every elements for CeO_2:Yb,Er@SiO_2@Ag UCNFs. As shown in Fig. S1a, XRD presents the characteristic peaks at 28.5°, 33.1°, 47.5°, and 56.5° with respective lattice planes (111), (200), (220), and (311), which are consistent with the cubic CeO_2. XPS spectra (Fig. S1b-d) indicated the existence of Er and Yb in the form of trivalent ions in CeO_2, cerium as all attributed to Ce^{4+} state [19,20], and a small amount of Ag simple substance.

https://doi.org/10.1016/j.jallcom.2018.07.225
0925-8388/

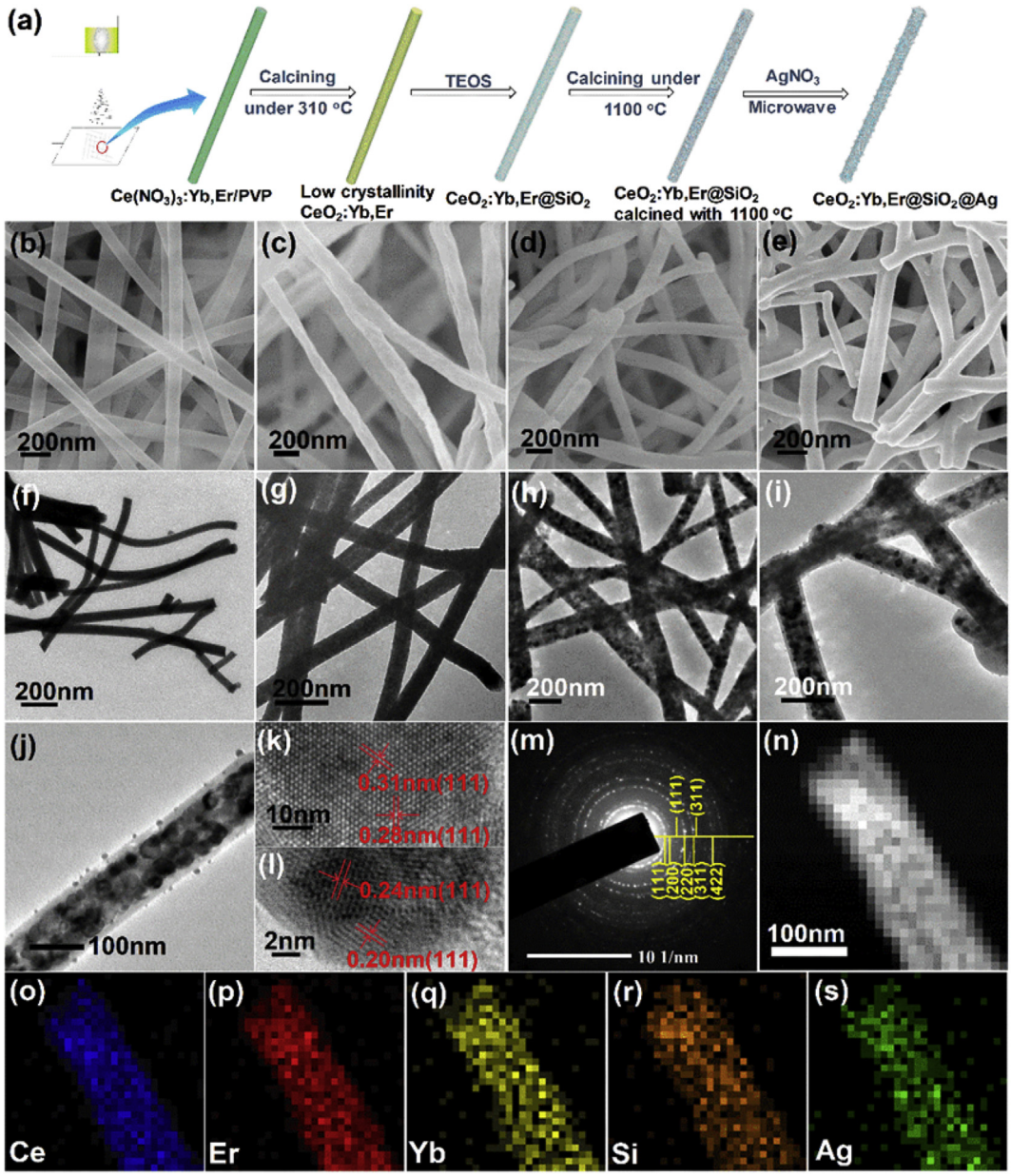

Fig. 1. (a) Illustration for the preparation of double-shell CeO_2:Yb,Er@SiO_2@Ag UCNFs. SEM and TEM images of (b) (f) precursor of CeO_2:Yb,Er nanofibers, (c) (g) CeO_2:Yb,Er nanofibers after 310 °C calcination, (d) (h) CeO_2:Yb,Er@SiO_2 nanofibers after 1100 °C calcination, and (e) (i) (j) CeO_2:Yb,Er@SiO_2@Ag UCNFs. (k) (l) HRTEM images, (m) SAED pattern, and (n) HAADF-STEM of CeO_2:Yb,Er@SiO_2@Ag UCNFs, element mapping images (o) Ce, (p) Er, (q) Yb, (r) Si, and (s) Ag.

In this case, the double-shell design could easily adjust the distance between fluorescence center and the outer layer of Ag NPs by controlling the thickness of the SiO_2 layer to achieve the maximum luminescence. When changing the amounts of TEOS, the different thickness of SiO_2 coating from 0 to 50 nm (Fig. S2) was synthesized. It is found that the bare CeO_2:Yb,Er nanofibers display faint upconversion luminescence. On the contrary, the CeO_2:Yb,Er@SiO_2 (15 nm) nanofibers show the highest emission intensity (Fig. 2), indicating the luminescence regulating effect of SiO_2 layer. Additionally, under the confinement effect of SiO_2 coating, the size of CeO_2:Yb,Er nanoparticles is about 40–50 nm (Fig. S2). However, it is clearly shown that the size of CeO_2:Yb,Er nanoparticles increases to 150 nm without the protection of SiO_2 shell (Fig. S3). The SiO_2 layers play two important roles in the CeO_2:Yb,Er@SiO_2@Ag UCNFs. On the one hand, the SiO_2 layers confine the growth and fusion of CeO_2:Yb,Er nanoparticles during the calcination process, which can enhance the scattering and collection of light; on the other hand, the crystal symmetry of CeO_2 is broken locally by binding of CeO_2 and SiO_2, and the asymmetry allows the f-f transitions in favor of upconversion luminescence property improvement [21,22].

Fig. S4a-b show the UV–vis absorption and Raman of CeO_2:Yb,Er, CeO_2:Yb,Er@SiO_2, and CeO_2:Yb,Er@SiO_2@Ag UCNFs. The coating of SiO_2 and loading of Ag NPs all improved the absorption for the whole wavelength and Raman effect. Under illumination of 980 nm laser (Fig. 3), the luminescence intensity of CeO_2:Yb,Er@SiO_2 (15 nm) nanofibers and CeO_2:Yb,Er@SiO_2@Ag UCNFs is 15 and 19 times stronger than CeO_2:Yb,Er at 550 nm in green emission spectra. The enhancement of luminescence intensity depends on the distance between fluorescence center and Ag NPs. The suitable distance between CeO_2:Yb,Er and Ag NPs can

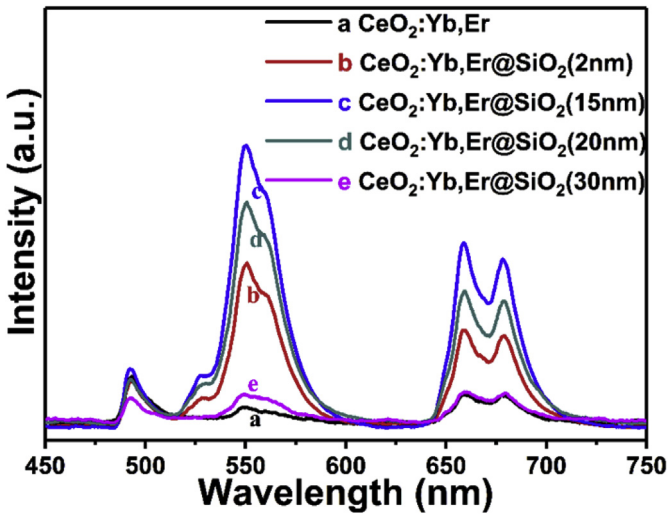

Fig. 2. Upconversion photoluminescence spectra of CeO_2:Yb,Er@SiO_2 nanofibers with different silica thickness: (a) without SiO_2, (b) ~ 2 nm, (c) ~15 nm, (d) ~20 nm, and (e) ~30 nm.

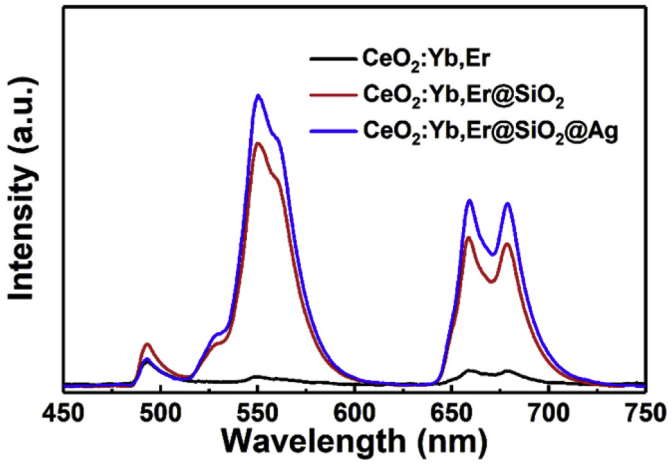

Fig. 3. Upconversion photoluminescence spectra of CeO_2:Yb,Er, CeO_2:Yb,Er@SiO_2 nanofibers, and CeO_2:Yb,Er@SiO_2@Ag UCNFs.

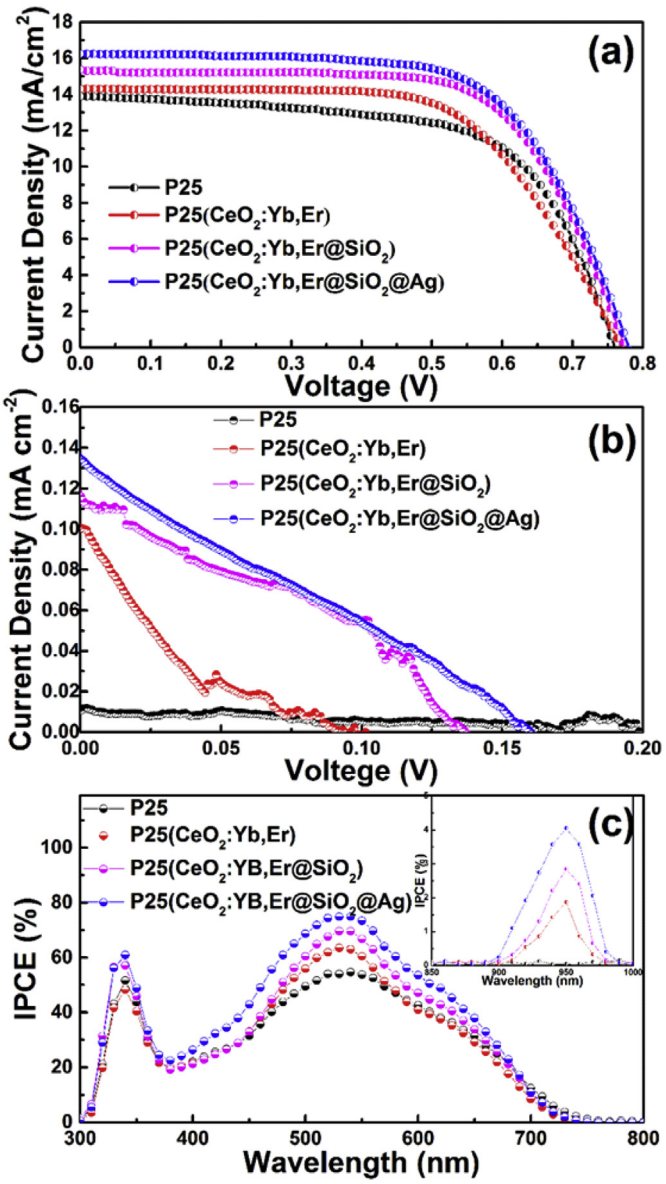

Fig. 4. The current density-voltage (*J-V*) characteristics of different fabrication DSSCs (a) under AM1.5G simulated sunlight irradiation (100 mW cm^{-2}) and (b) under 980 nm NIR laser, (c) IPCE curves of different fabrication DSSCs (inset is the IPCE curves of different fabrication DSSCs at the near-infrared wavelength from 850 to 1000 nm).

prevent the luminescence quenching. The nanoscale fluorophore-metal interactions give rise to the process called metal-enhanced fluorescence, which is caused by the interaction between excited fluorophores (CeO_2:Yb,Er) and surface plasmon resonance (SPR) of metals (Ag NPs).

To investigate the influence of UCNFs on DSSCs, we fabricated four kinds of DSSCs. CeO_2:Yb,Er, CeO_2:Yb,Er@SiO_2 nanofibers, and CeO_2:Yb,Er@SiO_2@Ag UCNFs were used as assistant layers, respectively. They are named as C1, C2 and C3, respectively. The control cell is normal DSSC (C4). Fig. 4a shows the photocurrent-voltage (*J-V*) characteristic of four DSSCs and the photovoltaic parameters listed in Table S1. The control cell displays a short current density (J_{sc}) of 13.99 mA cm^{-2}, $V_{oc} = 0.76$ V, $FF = 0.63$, and PCE = 6.65%. C3 shows a J_{sc} of 16.24 mA cm^{-2} and PCE of 8.17%, corresponding to enhancement for the 16.08% and 22.86%. C2 possess a J_{sc} of 15.32 mA cm^{-2} and PCE of 7.88%, the increase for the 9.5% and 18.49%; and C1 have a J_{sc} of 14.30 mA cm^{-2} and PCE of 6.89%.

To confirm the utilization of NIR light of the upconversion layer in DSSCs, the *J-V* curves of three DSSCs with upconversion assistant layer and normal DSSCs under 980 nm light were measured, as shown in Fig. 4b. It is clearly shown that the photocurrent for C4 is about close to zero, however, the DSSCs fabricated by CeO_2:Yb,Er based composite materials exhibit some photoresponse. Especially, CeO_2:Yb,Er@SiO_2@Ag UCNFs generated 0.135 mA cm^{-2} photocurrent. The above results confirmed that the enhancement of power conversion efficiency by double-shell CeO_2:Yb,Er@SiO_2@Ag UCNFs was predominantly due to the upconversion progress for broadband harvesting of NIR sunlight.

The incident photon-to-current conversion efficiency (IPCE) was investigated to further analyze the photovoltaic performance of four DSSCs, as shown in Fig. 4c. IPCE values of four DSSCs are increased in the order of P25 (CeO_2:Yb,Er@SiO_2@Ag) > P25 (CeO_2:Yb,Er@SiO_2) > P25 (CeO_2:Yb,Er) > P25. Under the assistance of double shells, i.e. SiO_2 layer and Ag NPs, C3 shows the highest IPCE value, which is ascribed to the upconversion ability of CeO_2:Yb,Er@SiO_2@Ag UCNFs. More interestingly, C1, C2, and C3 all showed an

improved broad-band NIR response at 900–1000 nm wavelength range (the inset of Fig. 4c), clearly corresponding to C4 without NIR response. Therefore, the upconversion assistant layers treated cell display broader light responses and higher IPCE values owing to superior upconversion luminescence ability.

4. Conclusion

In summary, double-shell CeO_2:Yb,Er@SiO_2@Ag upconversion composite nanofibers were successfully synthesized by a multi-step process. CeO_2:Yb,Er@SiO_2@Ag UCNFs show the excellent upconversion luminescence property. The increase of luminescence intensity should be attributed to the following three factors: (1) the SiO_2 coatings act the role of light enrichment, and break the crystal symmetry of CeO_2 and allow f-f transitions, which result in the improved upconversion property; (2) Ag NPs display the SPR effect, which further increases upconversion property of CeO_2:Yb,Er; (3) the SiO_2 layers provide an adjustable distance between fluorescence center and Ag NPs to prevent the luminescence quenching. When CeO_2:Yb,Er@SiO_2@Ag were used as an assistant layer in DSSCs, the PCE was higher than normal cells. This work widens the light absorption range of DSSCs, improves the utilization ratio of solar light, and provides a feasible scheme for increasing the efficiency of DSSCs photoelectric conversion.

Acknowledgement

This work was financially supported by the National Natural Science Foundation of China (Grant No. 21773203) and the Natural Science Foundation of Jiangsu Province (BK20161329).

Appendix A. Supplementary data

Supplementary data related to this article can be found at https://doi.org/10.1016/j.jallcom.2018.07.225.

References

[1] B. O'Regan, M. Graetzel, Nature 353 (1991) 737–740.
[2] Z. Hosseini, N. Taghavinia, E.W.G. Diau, Mater. Lett. 188 (2017) 92–94.
[3] F. Wu, X. Li, Y. Tong, T. Zhang, J. Power Sources 342 (2017) 704–708.
[4] X.Y. Huang, J. Alloys Compd. 690 (2017) 356–359.
[5] M.M. Guo, H.M. Yang, X. Jian, J.G. Li, Z.H. Liang, P.D. Han, Appl. Surf. Sci. 428 (2018) 851–860.
[6] G. Chen, J. Damasco, H. Qiu, W. Shao, T.Y. Ohulchanskyy, R.R. Valiev, X. Wu, G. Han, Y. Wang, C. Yang, H. Agren, P.N. Prasad, Nano Lett. 15 (2015) 7400–7407.
[7] Y. Huang, H. Xu, H. Yang, Y. Lin, H. Liu, Y. Tong, ACS Sustain. Chem. Eng. 6 (2018) 2751–2757.
[8] Y. Huang, K. Li, Y. Lin, Y. Tong, H. Liu, ChemCatChem 10 (2018) 1982–1987.
[9] J.H. Wu, J.L. Wang, J.M. Lin, Z. Lan, Q.W. Tang, M.L. Huang, Y.F. Huang, L.Q. Fan, Q.B. Li, Z.Y. Tang, Adv. Energy Mater. 2 (2012) 78–81.
[10] J. Wang, Y. Niu, M. Hojamberdiev, F.M. Alamgir, Y. Cai, K. Jacob, Sol. Energy Mater. Sol. Cell. 160 (2017) 361–371.
[11] N. Yao, J. Huang, K. Fu, X. Deng, M. Ding, M. Shao, X. Xu, Electrochim. Acta 154 (2015) 273–277.
[12] R. Rajeswari, K. Susmitha, C.K. Jayasankar, M. Raghavender, L. Giribabu, Sol. Energy 157 (2017) 956–965.
[13] H. Lu, W. Fan, Y. Huang, T. Liu, Nano Res. 11 (2018) 1274–1284.
[14] Y.M. Liu, Y. Xia, Y. Jiang, M.L. Zhang, W.W. Sun, X.Z. Zhao, Electrochim. Acta 180 (2015) 394–400.
[15] R.F. Zhao, L. Huan, P. Gu, R. Guo, M. Chen, G.W. Diao, J. Power Sources 331 (2016) 527–534.
[16] J.Y. Bai, R.F. Zhao, G. Han, Z.C. Li, G.W. Diao, RSC Adv. 5 (2015) 43328–43333.
[17] Y. Huang, B. Long, M. Tang, Z. Rui, M.-S. Balogun, Y. Tong, H. Ji, Appl. Catal. B Environ. 181 (2016) 779–787.
[18] Y. Huang, H. Li, M.-S. Balogun, H. Yang, Y. Tong, X. Lu, H. Ji, RSC Adv. 5 (2015) 7729–7733.
[19] B.M. Reddy, A. Khan, Y. Yamada, T. Kobayashi, S. Loridant, J.C. Volta, J. Phys. Chem. B 107 (2003) 5162–5167.
[20] S.H.O.D.R. Mullins*, D.R. Huntley, Surf. Sci. 409 (1998) 307–319.
[21] G. Guo, Y. Guo, H. Tan, H. Yu, W. Chen, E. Fong, Q. Yan, J. Mater. Chem. 4 (2016) 10893–10899.
[22] J. Shen, Z.Q. Li, Y.R. Chen, X.H. Chen, Y.W. Chen, Z. Sun, S.M. Huang, Appl. Surf. Sci. 270 (2013) 712–717.

Rongfang Zhao
School of Chemistry and Chemical Engineering, Yangzhou University, Yangzhou 225002, PR China

Yantai Institute of Coastal Zone Research, Chinese Academy of Sciences, Yantai 264003, PR China

Qianhui Wu
School of Chemistry and Chemical Engineering, Yangzhou University, Yangzhou 225002, PR China

Dongmei Tang
School of Chemistry and Chemical Engineering, Yangzhou University, Yangzhou 225002, PR China

Wenlong Li
School of Chemistry and Chemical Engineering, Yangzhou University, Yangzhou 225002, PR China

Xiue Zhang
School of Chemistry and Chemical Engineering, Yangzhou University, Yangzhou 225002, PR China

Ming Chen*
School of Chemistry and Chemical Engineering, Yangzhou University, Yangzhou 225002, PR China

Rong Guo
School of Chemistry and Chemical Engineering, Yangzhou University, Yangzhou 225002, PR China

Guowang Diao**
School of Chemistry and Chemical Engineering, Yangzhou University, Yangzhou 225002, PR China

* Corresponding author.

** Corresponding author.
E-mail address: chenming@yzu.edu.cn (M. Chen).
E-mail address: gwdiao@yzu.edu.cn (G. Diao).

30 May 2018
18 July 2018
19 July 2018
Available online 23 July 2018